


# Modeling the Impact of Temperature on the Electrical Activity of Cardiac Cells: Identification of Key Ionic Currents

V. O. Ivashchuk<sup>f</sup>,  [0009-0004-2687-9188](https://orcid.org/0009-0004-2687-9188)

N. H. Ivanushkina<sup>s</sup>, PhD., Assoc.Prof.,  [0000-0001-8389-7906](https://orcid.org/0000-0001-8389-7906)

Department of Electronic Engineering

National Technical University of Ukraine "Igor Sikorsky Kyiv Polytechnic Institute",  [00syn5v21](https://www.researchgate.net/profile/Vladimir-Ivashchuk)  
Kyiv, Ukraine

**Abstract**—This study presents the development of a modified electrophysiological model of a human epicardial cardiomyocyte, achieved by taking into account the temperature effects on the kinetics and conductance of ion channels using parameter-specific Q10 coefficients. Based on the modified model, a temperature sensitivity analysis was performed to identify the key ionic mechanisms that regulate thermal adaptation of action potential duration (APD). The simulation was performed in the temperature range of 25–45 °C using a hybrid approach that combines local and global sensitivity analyses. Local analysis was performed by calculating elasticity coefficients to evaluate the impact of individual temperature parameters on APD. Global analysis was carried out using the Morris method of elementary effects to rank parameters by their influence and to identify non-linear interactions. The results demonstrate that the rapid delayed rectifier potassium current (IKr) plays a predominant role in the modulation of APD. It accounts for approximately 85% of the total APD shortening when the temperature rises to 42 °C, where APD decreases by 22.03% (from 270.91 ms to 211.24 ms). Under deep hypothermia (25 °C), a 52.47% prolongation of the action potential (AP) and a 169% increase in the repolarization phase duration were observed. Furthermore, the study reveals that at moderate hypothermia (30 °C), non-linear interactions between various ion channels become a decisive factor. A significant contribution of the sodium-calcium exchanger (NCX) and the late sodium current (INaL) was demonstrated at lower temperatures, confirming the temperature dependence of these interactions. These findings underscore the critical role of the human Ether-à-go-go-Related Gene (hERG) in the thermal adaptation of the ventricular myocardium and provide a computational framework for investigating the mechanisms of thermo-induced arrhythmias.

**Keywords** — temperature effects; cardiac electrophysiology; sensitivity analysis; Morris method; temperature coefficients Q10; action potential; ion channels.

## I. INTRODUCTION

Temperature exerts a deep influence on the morphology and characteristics of cardiomyocyte action potentials (AP), specifically affecting action potential duration (APD), the maximum rate of depolarization ( $(dV/dt)_{max}$ ), the resting membrane potential ( $V_{rest}$ ), and other electrophysiological parameters[1]. Along with its independent effect on the cardiac conduction system, thermal stress exhibits synergism with pathological factors such as impaired ionic homeostasis and hypoxia, which significantly increases the risk of ventricular fibrillation [2]. Understanding these processes is critical for assessing the physiological state under temperature fluctuations or during clinical procedures involving thermal effects on cells. A prime example is radiofrequency ablation (RFA), which employs high temperatures ( $\geq 50$  °C) to destroy pathological myocardial regions, directly altering the electrophysiological properties of cardiomyocytes [3].

Recent meta-analyses and global epidemiological studies indicate a direct correlation between environmental temperature fluctuations and an increased risk of cardiovascular complications. It has been established that every 1 °C rise in ambient temperature significantly raises cardiovascular mortality rates, while prolonged heatwaves correlate with a mortality increase of  $\approx 17\%$ , particularly among patients aged over 65 years[4]. Such a statistical correlation underscores the urgent need for a detailed study of the ionic mechanisms underlying myocardial thermal adaptation, because thermal stress can act as a trigger for fatal rhythm disturbances.

Contemporary research relies not only on experimental data but also on mathematical models validated *in vivo* and *in vitro*. One of the most advanced mathematical models of human cardiac electrophysiology is the ToR-ORd (Tomek–O'Hara–Rudy, 2019) model[5]. Unlike the O'Hara–Rudy (2011) model, this version features a refined description of potassium channel kinetics



and intracellular calcium dynamics. Since these channels exhibit high temperature sensitivity [6], [7], the ToR-ORd model is the most suitable for investigating thermal effects. However, the original model is calibrated for a stable temperature of 37 °C, which limits its applicability in scenarios where temperature is a variable factor.

Among the mechanisms underlying the temperature dependence of cardiac cells, ion-channel modulation remains the most extensively studied. Temperature variations affect ion diffusion rates, activation and inactivation kinetics, and biochemical processes involved in transmembrane transport [1]. However, despite a significant amount of research focused on individual channels, many ionic currents and their combined temperature-dependent interactions remain insufficiently characterized, especially in human ventricular cell models. Therefore, the incorporation of extrapolated experimental data and approximated  $Q_{10}$  coefficients is necessary for processes where direct human data are unavailable [8]. This approach allows for extending the model's capabilities by accounting for temperature effects across a wide range of ionic currents.

Although modern electrophysiological models of human cardiomyocytes provide detailed descriptions of ionic currents and calcium handling, their thermal component remains insufficiently developed. Previous studies have often relied on older models with simplified calcium and potassium dynamics, and there is still no systematic analysis of the temperature dependence of the human-based ToR-ORd model that would quantify the contribution of individual currents and nonlinear interactions to AP formation under hypo- and hyperthermic conditions. Therefore, the aim of this study is to develop a temperature-modified version of the ToR-ORd model using  $Q_{10}$  coefficients and to identify the key ionic mechanisms responsible for AP thermal adaptation through sensitivity analysis.

## II. MATERIALS AND METHODS

### A. General Research Framework

The study is based on the modification of a mathematical model and the analysis of its sensitivity to thermal effects.

The research framework consisted of three consecutive stages. First, a temperature-dependent version of the ToR-ORd model was developed by incorporating  $Q_{10}$  coefficients into the descriptions of ion-channel conductance and kinetics. Second, simulation protocols were applied to verify the electrophysiological behavior of the modified model and to perform local and global sensitivity analyses. Finally, the obtained results were statistically processed and interpreted to rank the temperature-sensitive parameters and identify the key ionic mechanisms involved in AP thermal adaptation.

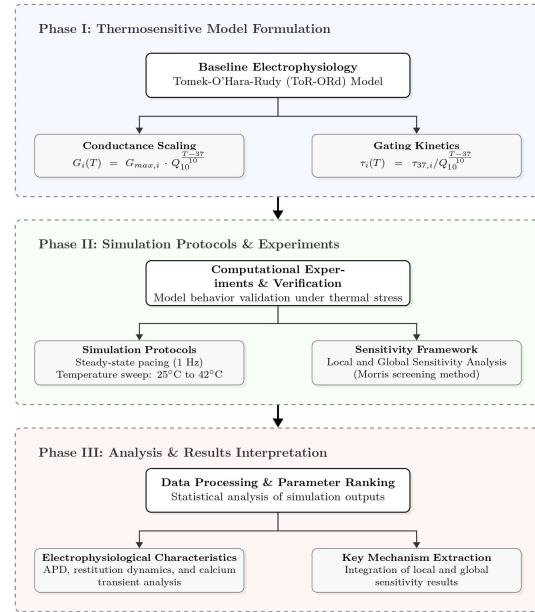


Fig. 1 Methodological workflow of the *in silico* study. The pipeline is divided into three main phases: I) integration of thermosensitive parameters into the model; II) execution of simulation protocols and experiments; III) analysis and result interpretation.

The general framework of the research algorithm is shown in Fig. 1.

### B. Mathematical Model of Cardiac Cell Electrical Activity

The study is based on the ToR-ORd mathematical model [5], which describes the electrophysiology of the ventricular myocyte. The evolution of the membrane potential  $V_m$  is described by the classical current balance equation, where the rate of change of the potential is determined by the difference between the external stimulus current and the total transmembrane ionic current:

$$C_m \frac{dV_m}{dt} = -(I_{ion} - I_{stim}),$$

where  $C_m$  is specific membrane capacitance,  $I_{stim}$  is applied stimulus current,  $I_{ion}$  is aggregated current encompassing contributions from ion channels, pumps, and exchangers.

Within the scope of this work,  $I_{ion}$  was decomposed into its individual components to facilitate the introduction of temperature dependence using  $Q_{10}$  coefficients, which modulate both the maximum conductances/permeabilities and the kinetic gating parameters. Depending on the current formulation, these kinetic parameters include the time constants of activation and inactivation gates, for example  $\tau_m$ ,  $\tau_h$ ,  $\tau_j$  for  $I_{Na}$ ;  $\tau_{mL}$  and  $\tau_{hL}$  for  $I_{NaL}$ ;  $\tau_d$ ,  $\tau_f$ , and  $\tau_{fCa}$

-related constants for  $I_{CaL}$ ;  $\tau_{xs1}$  and  $\tau_{xs2}$  for  $I_{Ks}$ ; and  $\tau_a / \tau_i$  -related constants for  $I_{to}$ . For Markov-type descriptions, such as IKr, temperature scaling was applied to the corresponding transition rate constants rather than to a single time constant.

### C. Temperature Integration in the Model

The ToR-ORd model was modified using  $Q_{10}$  coefficients to account for the temperature dependence of key ionic conductances and kinetics. The application of the  $Q_{10}$  temperature coefficient is based on the empirically established exponential relationship between temperature and both the rate constants (kinetics) and the maximum conductance of ion channels. This approach serves as a biological interpretation of the Arrhenius equation, which describes the activation energy required for the conformational transitions of channel protein molecules during their switching between functional states [9].

The temperature effect on the modified model parameters is determined using an exponential factor  $k_T$ , which is calculated relative to a reference temperature

$$T_{ref} = 37 \text{ }^\circ\text{C (or 310.15,K):}$$

$$T_{exp} = \frac{(T - T_{ref})}{10},$$

$$k_T = Q_{10}^{T_{ref}},$$

where  $T$  is current temperature,  $Q_{10}$  is process-specific coefficient that defines the change in reaction rate for every 10 °C change in temperature.

All  $Q_{10}$  coefficients are dimensionless.

For ion channels, pumps, and exchangers, the temperature correction of the current amplitude is performed by scaling the maximum conductance ( $G$ ) or permeability ( $P$ ):

$$G(T) = G_{ref} \cdot k_T,$$

$$P(T) = P_{ref} \cdot k_T,$$

where  $G_{ref}$ ,  $P_{ref}$  are initial conductance and permeability, respectively.

The temperature effect on the kinetics of channel opening and closing is taken into account in two ways, depending on the formulation of the equations in the model:

- If the kinetics are described using time constants ( $\tau$ ), an increase in temperature accelerates the processes, leading to a decrease in the time constants:

$$\tau(T) = \frac{\tau_{ref}}{k_T},$$

- where  $\tau_{ref}$  represents the functions describing the ion channel time constants.
- If the kinetics is defined from rate constants (as in Markov models), they are scaled directly:

$$\alpha(T) = \alpha_{ref} \cdot k_T,$$

$$\beta(T) = \beta_{ref} \cdot k_T,$$

- where  $\alpha_{ref}$ ,  $\beta_{ref}$  are functions describing the opening and closing rates of the ion channels, respectively.

$Q_{10}$  coefficients were selected from literature sources using a hierarchical approach, prioritizing experimental data obtained from human cells. When such data were unavailable, alternative well-established values from the literature were adopted, which introduces an additional source of variability (e.g., Sarcoplasmic/Endoplasmic Reticulum Ca<sup>2+</sup>-ATPase (SERCA), Na-K pump). The  $Q_{10}$  values used for the primary model components are summarized in table 1.

### D. Simulation and Analysis Protocol

The investigated temperature range (25–45 °C) is determined by the physicochemical constraints of biological structures and the specificity of available experimental data. The lower bound (25 °C) corresponds to the conditions of most patch-clamp ion channel studies, as lower temperatures often lead to technical instability of cellular membranes [22], [23]. The upper bound (45 °C) is defined by the thermal denaturation threshold of protein structures. Beyond these limits, the system's behavior changes fundamentally and requires description via Macromolecular Rate Theory (MMRT) instead of the exponential  $Q_{10}$  approach [24], [25].

For the numerical simulation of the model, the specialized Myokit library (v.1.33) [26] in Python was utilized. Since the model is described by a stiff system of ordinary differential equations (ODEs), the CVODE (C-language Variable-coefficient Ordinary Differential Equation solver) integrator from the SUNDIALS (SUite of Nonlinear and Differential/ALgebraic equation Solvers) [27] was employed. This tool is specifically optimized for solving systems characterized by a significant disparity in the time scales of the underlying processes.

Since the establishment of ionic homeostasis (particularly for  $[Na^+]_i$  and  $[Ca^{2+}]_i$  concentrations) is a prolonged process, a pre-simulation was performed to stabilize the model before each calculation. The stabilization criterion was defined as a relative change in the sodium ion concentration at the end of a cycle which did not exceed 0.001%. To satisfy this requirement, a protocol of 2000 preparatory cycles (1 s each) was established in accordance with current standards in biophysical research [28], [29].



TABLE 1  $Q_{10}$  TEMPERATURE COEFFICIENTS FOR THE PRIMARY COMPONENTS OF THE TOR-ORD MODEL.

Functional System	Parameter Group	Model parameter	Value (Q10)	Source
Sodium Currents	Fast $I_{Na}$ Conductance	Q10_GNa	1.4	[10]
	Fast $I_{Na}$ Activation	Q10_INa_m/h	2.0 / 2.0	[11]
	Fast $I_{Na}$ Inactivation	Q10_INa_j	3.1	[12]
Potassium Currents	Late $I_{NaL}$ Conductance	Q10_GNaL	1.5	[13]
	Late $I_{NaL}$ Kinetics	Q10_INaL_kinetics	2.0	[13]
	Rapid Rectifier ( $I_{Kr}$ )	Q10_GKr	2.1	[14]
	$I_{Kr}$ Gating Kinetics	Q10_IKr_xr_fast/slow	4.69 / 4.55	[14]
	Slow Rectifier ( $I_{Ks}$ )	Q10_GKs	3.11	[15]
Calcium Dynamics	$I_{Ks}$ Activation	Q10_IKs_xs	4.9	[15]
	Inward Rectifier ( $I_{K1}$ )	Q10_GK1 / kinetics	1.8 / 3.9	[16]
	Transient Outward ( $I_{to}$ )	Q10_Gto	1.23	[17]
	$I_{to}$ Gating	Q10_Ito_a/i	1.76 / 4.2	[17]
	L-Type Permeability	Q10_PCaL	1.5	Passive aqueous diffusion (assumption)
	$I_{CaL}$ Gating (VDI/CDI)	Q10_ICaL_d/f/fCa	2.1	[18]
	SERCA Pump	Q10_Jup	3.13	[19]
Active Transport	$Na^+ / K^+$ Pump	Q10_NaK	1.87	[20]
	$Na^+ / Ca$ Exchanger	Q10_NCX	2.6	[21]
Background & Others	Leak Currents	Q10_GbNa / GbCa	1.5/1.5	Passive aqueous diffusion (assumption)

The following parameters were used to evaluate the functional state of the model:

- Resting Membrane Potential ( $V_{rest}$ ): The value of the membrane potential at steady state prior to stimulation.

- $(dV/dt)_{max}$ : The peak value of the time derivative of the membrane potential during phase 0 (depolarization).
- Action Potential Amplitude (APA): The difference between the maximum depolarization peak and the  $V_{rest}$  level.
- Action Potential Duration (APD): The time interval from the moment of maximum depolarization rate to 50% (APD50) and 90% (APD90) repolarization of the amplitude. APD90 is the primary indicator of total APD.
- Repolarization Morphological Index (RMI): Defined as the time interval between 50% and 90% repolarization (APD90 – APD50).
- Calcium Transient Amplitude ( $[Ca^{2+}]_i$ ): Defined as the difference between the peak (systolic) and baseline (diastolic) concentrations of free cytosolic calcium during a single cardiac cycle.

#### E. Combined Approach Based on Local and Global Sensitivity Analysis

To investigate the mechanisms of thermal adaptation in detail, a combined approach was employed, integrating local and global sensitivity analysis methods.

The local analysis is based on the calculation of elasticity coefficients  $E_{param}$  [30]. This approach allows for the assessment of the relative contribution of each individual temperature coefficient to the change in APD. Since the baseline value of the factor  $k_T$  at 37 °C is equal to unity, the expression  $(Q_{10,param} - 1)$  reflects the relative variation of the parameter for a 10 °C step. The calculation is performed using the following formula:

$$E_{param} = \frac{(APD_{iso} - APD_{ref}) / APD_{ref}}{Q_{10,param} - 1},$$

where  $APD_{iso}$  is APD obtained through the isolated activation of a specific temperature coefficient;  $APD_{ref}$  is the reference APD at 37 °C;  $Q_{10,param}$  is the value of the corresponding temperature coefficient from table 1.

To fully elucidate the nature of thermal sensitivity, simulations were performed under three complementary scenarios. In the first scenario, all  $Q_{10}$  coefficients were activated simultaneously to evaluate the total integrated temperature response of the model. In the second scenario, temperature dependence was applied only to the Nernst equations, while all  $Q_{10}$  coefficients were fixed at unity, allowing the passive thermodynamic contribution to be isolated. In the third scenario, each  $Q_{10}$  coefficient was activated individually while maintaining the temperature dependence of the Nernst equations,

which made it possible to estimate the isolated contribution of each ionic mechanism.

$E_{param}$  is calculated specifically for this scenario to identify the isolated contribution of each channel.

Global sensitivity analysis was conducted using the Morris elementary effects method [31] for 30 °C and 42 °C regimes. This method allows for exploring the parameter space beyond the local neighborhood of the reference point and assessing nonlinear interactions. For 28 parameters, a variation range of  $\pm 30\%$  from their baseline values was established. The number of trajectories ( $r = 100$ ) (totaling 2,900 simulations per scenario) ensured high coverage density of the parameter space  $Q_{10}$ .

Statistical processing of the results included the calculation of two key indices:

- $\mu^*$  (Mean of the absolute elementary effects): The average of the absolute values of the elementary effects. This index serves as an integral measure of the overall significance (importance) of a parameter. A high value indicates that the investigated ionic mechanism plays a key role in APD90 variability during temperature changes and is a determining factor in myocardial thermal adaptation.
- $\sigma$  (Standard deviation of the elementary effects): This index acts as a measure of the model's response nonlinearity. A high value suggests that the influence of a given  $Q_{10}$  changes significantly depending on the values of other parameters, indicating the presence of synergistic or antagonistic interactions between ion channels.

#### F. Visualization and Statistical Decomposition Methods

To provide a comprehensive interpretation of the simulation results and to reveal the structure of nonlinear interactions between ionic components, several complementary visualization and statistical decomposition methods were applied.

First, contribution decomposition was used to separate the total temperature-induced change in APD90 into individual linear contributions associated with specific ionic currents and a residual nonlinear interaction term. This approach made it possible to quantify the relative role of each temperature-dependent mechanism in APD90 prolongation or shortening and to estimate the contribution of synergistic or antagonistic interactions that cannot be explained by isolated parameter effects alone.

The results of global sensitivity analysis were additionally represented in the Morris parameter space using scatter plots in "influence–interaction" coordinates. In

this representation, the mean of the absolute elementary effects,  $\mu^*$ , characterizes the overall influence of a given  $Q_{10}$  coefficient on APD90, whereas the standard deviation,  $\sigma$ , reflects the degree of nonlinearity and the intensity of its interaction with other model parameters. Therefore, parameters with high  $\mu^*$  and low  $\sigma$  were interpreted as dominant but relatively independent regulators of APD90, while parameters with simultaneously high  $\mu^*$  and high  $\sigma$  were considered nonlinear modulators whose effects strongly depend on the state of other ionic mechanisms.

To compare the relative importance of the temperature-sensitive parameters under different thermal conditions, hierarchical ranking diagrams were constructed using the Morris  $\mu^*$  index. These diagrams allowed the identification of dominant target mechanisms under hypothermic and hyperthermic conditions and made it possible to assess whether the same ionic currents preserve their regulatory role across different temperature regimes. In addition, heatmap visualization was used to represent the direction and magnitude of individual  $Q_{10}$ -dependent contributions over the investigated temperature range, thereby illustrating the transition from APD90 prolongation during cooling to APD90 shortening during heating.

Finally, phase portraits of intracellular calcium concentration versus membrane potential were constructed to evaluate temperature-dependent changes in electro-mechanical coupling. These hysteresis-like loops were used to analyze the temporal relationship between membrane excitation and the calcium transient during the action-potential cycle. Changes in the width, compression, and orientation of the phase loops were interpreted as indicators of altered synchronization between electrical activation and intracellular calcium handling under hypo- and hyperthermic conditions.

### III. RESULTS

#### A. Temperature Dependence of the Model's Electrophysiological Characteristics.

As a result of the simulation, the time dependences of the AP and calcium transient in the temperature range of 25 to 45 °C were obtained (Fig. 2). Under deep hypothermia (25 °C) APD90 increased by 52.47% compared to the baseline level (37 °C), reaching 413.07 ms. The RMI parameter increased by 169% (from 49.78 ms to 133.92 ms), indicating a significant slowing of the final repolarization phase.

Excitability parameters also underwent changes. At 25 °C,  $V_{rest}$  shifted toward depolarization by 4.8 mV (to  $-84.21$  mV). Despite the resting potential's approach to the activation threshold,  $(dV/dt)_{max}$  decreased



by 37.51% (to 59.77 V/s). The observed APD90 prolongation correlates with experimental findings on isolated human heart preparations, where hypothermia was reported to cause similar AP lengthening due to a marked reduction in the conductances of the rapid and slow components of the delayed rectifier potassium current ( $I_{Kr}$  and  $I_{Ks}$ ) [32]. The dynamics of change in the model agree with experimental trends, although absolute duration values may vary within a range of 5–12%.

Under hyperthermia (42 °C), APD90 decreased by 22.03% (to 211.24 ms), while  $(dV/dt)_{\max}$  simultaneously increased to 111.17 mV/ms (Fig. 3). This aligns with clinical data, where QT interval shortening is a typical marker of tachyarrhythmia risk during fever [32]. The formation of a hyperexcitable state alongside a shortened refractory period creates a substrate for *re-entry* mechanisms [33].

Particular attention should be paid to the calcium transient amplitude  $[Ca^{2+}]_i$ , which exhibits a nonlinear behavior with a minimum around 34 °C (Fig. 2). At 25 °C, the peak  $[Ca^{2+}]_i$  concentration increased by 78.8% (to 0.69  $\mu\text{M}$ ), whereas at 42 °C, the increase was moderate (+13.6%, 0.44  $\mu\text{M}$ ). The increase in calcium transient amplitude during cooling is a classic effect in cardiac physiology, attributed to the altered balance between the Na-Ca exchanger (NCX) and SERCA pump activities [34].

The characteristic minimum below the physiological norm (37 °C) is a specific feature of this model. This may suggest that the optimal balance between the capture rate of calcium by the SERCA pump and its release via ryanodine receptors (RyR) is achieved specifically within the range of moderate hypothermia (33–35 °C). Such a state underlies the protective effect of targeted temperature management (32–34 °C) following ischemia [35]. However, it is noteworthy that recent clinical studies on temperature effects demonstrate similar efficacy for milder cooling ( $\approx 36$  °C), questioning the exclusivity of the narrow "therapeutic window" of 32–34 °C [35].

### B. Model Sensitivity Analysis

Local sensitivity analysis of individual temperature-dependent parameters identified the key ion channels that exert a predominant influence on AP duration in the model. (Fig. 4) presents the decomposition of contributions from various parameters to the change in APD90. The results indicate the presence of nonlinear interactions among AP components within the model: while their total synergistic contribution is negligible at 42 °C, the residual term (nonlinear interaction) becomes prominent at 30 °C. This suggests a complex synergy between ionic components under hypothermic conditions.

Analysis of individual parameter contributions demonstrated a reversal in the sign of the effect when

shifting from 30 °C to 42 °C relative to the reference point of 37 °C. This occurs because the  $k_T$  factor alters the process dynamics depending on the direction of the temperature deviation. At 30 °C, the high thermal sensitivity  $Q_{10}$  for the  $I_{Kr}$  current leads to a substantial prolongation, with  $\Delta\text{APD} = +67.1$  ms, because cooling inhibits the outward potassium flux. Conversely, at 42 °C, the same parameter becomes the primary driver of AP shortening, with a 42.3 ms reduction in APD90 due to accelerated repolarization.

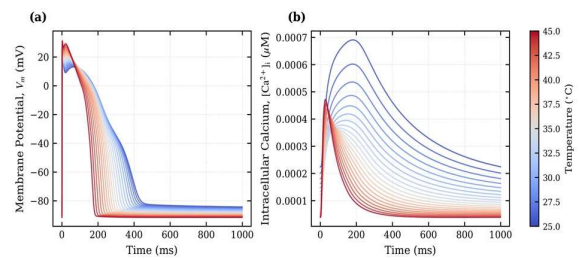


Fig. 2 Temperature-dependent waveforms generated by the  $Q_{10}$ -modified ToR-ORd model: a) AP; b) calcium transient.

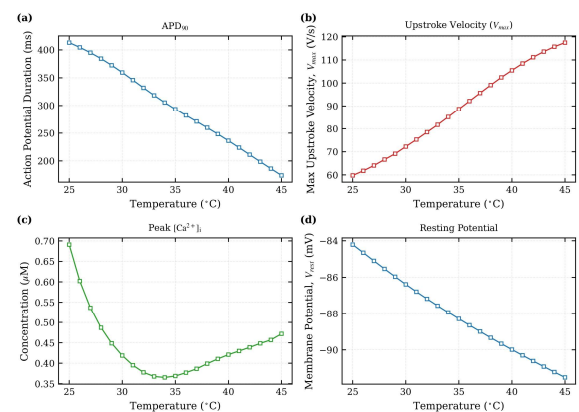


Fig. 3 Temperature dependence of key electrophysiological characteristics: a) APD90 (ms); b) resting membrane potential  $V_{rest}$  (mV); c) maximal upstroke velocity  $(dV/dt)_{\max}$  (V/s); d) peak intracellular  $[Ca^{2+}]_i$  ( $\mu\text{M}$ ).

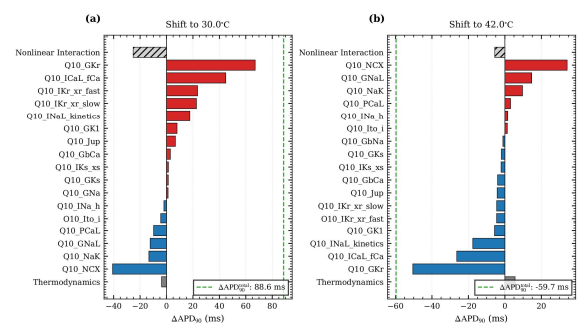


Fig. 4 Waterfall decomposition of total APD90 into linear contributions from individual  $Q_{10}$  parameters and the nonlinear interaction residual: a) at 30 °C; b) at 42 °C. (Positive/negative bars show prolongation/shortening of APD90).



The influence of  $Q_{10}$  for the NCX at 30 °C contributes to AP shortening, producing a 40.8 ms reduction in APD90, whereas at 42 °C it contributes to APD prolongation, with  $\Delta APD = +34.1$  ms. A similar behavior

is observed for  $I_{NaL}$ , where the effect shifts from a 12.4 ms reduction in APD90 under hypothermia to a 14.7 ms increase under hyperthermia (Fig. 5).

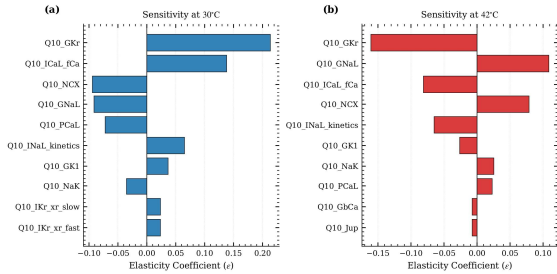


Fig. 5 Sensitivity ranking based on elasticity coefficients: relative contributions of temperature-dependent parameters to APD90 modulation: a) at 30 °C; b) at 42 °C. (higher values = greater impact).

To visualize the relative influence of individual parameters on APD across different temperatures, a heatmap of their contributions was generated (Fig. 6).

For a detailed analysis of the model's global sensitivity and nonlinearity, the Morris method was applied. This approach facilitated the ranking of parameters based on the mean of the absolute elementary effects ( $\mu^*$ ), which determines the overall importance of a parameter, and the standard deviation of the elementary effects ( $\sigma$ ), which serves as a measure of response nonlinearity and the presence of inter-parameter interactions (Fig. 7).

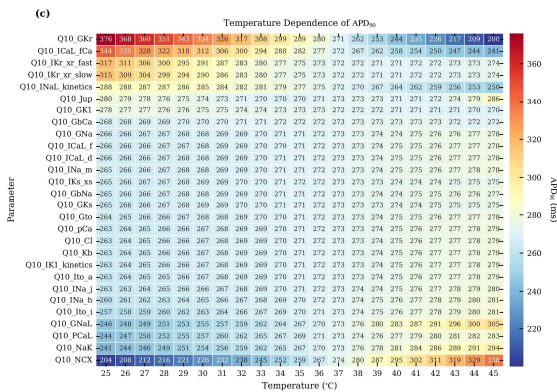


Fig. 6 Heatmap of individual  $Q_{10}$  parameter contributions to APD90 change across 25–45 °C.

According to the Morris index  $\mu^*$  (Fig. 8), the largest contributions to APD90 variability under both temperature regimes are attributed to:

1.  $Q_{10}$  for the conductance of rapid delayed rectifier potassium channels ( $G_{Kr}$ ):  $\mu^* = 51,9$  at 30 °C and  $\mu^* = 36,75$  at 42 °C.
2.  $Q_{10}$  for NCX:  $\mu^* = 38,7$  at 30 °C and  $\mu^* = 19,8$  at 42 °C.
3.  $Q_{10}$  for the calcium-dependent inactivation of L-type calcium channels ( $f_{Ca}$ ):  $\mu^* = 16,65$  at 30 °C and  $\mu^* = 25,5$  at 42 °C.

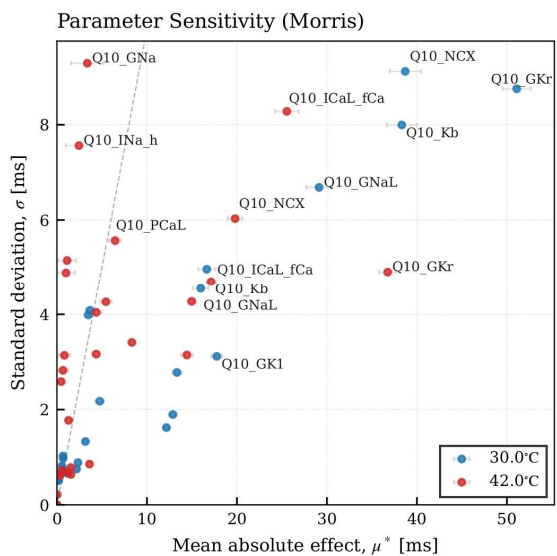


Fig. 7 Morris sensitivity analysis of model parameters at 30 °C and 42 °C. The scatter plot displays the  $\sigma$  vs  $\mu^*$ . Parameters with higher  $\mu^*$  indicate greater overall influence on APD90, while higher  $\sigma$  values signify increasing nonlinearity or complex interactions with other model components.

Analysis of the  $\sigma$  indices revealed a shift in the nature of nonlinearity depending on the thermal regime. At 42 °C, a "destabilization" of the fast sodium channels is observed:  $\sigma$  for these parameters exceeds  $\mu^*$  by 2,5–3 times, indicating the emergence of complex interactions between the depolarization phase and other currents. Conversely, the  $I_{Kr}$  parameters exhibit a consistently high  $\mu^*$  with a low  $\sigma$ , positioning it as an independent factor influencing APD.

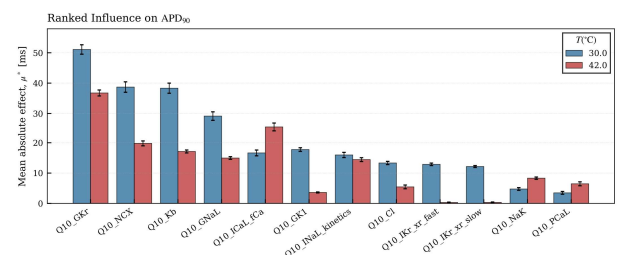


Fig. 8 Hierarchical ranking of dominant  $Q_{10}$  parameters in the model based on Morris  $\mu^*$  index under hypothermic and hyperthermic conditions.



The redistribution of nonlinearity among calcium-handling components is of particular interest. At 30 °C, high nonlinearity is observed for  $P_{CaL}$  (L-type channel permeability) and NCX, suggesting a high interdependence of calcium homeostasis processes during cooling. Upon heating to 42 °C, these parameters become more "linear," while the primary nonlinearity shifts toward  $I_{NaL}$ , which may explain the increased susceptibility to arrhythmias during critical hyperthermia.

### C. Restitution Dynamics and Phase Analysis of Electromechanical Coupling

To perform an in-depth analysis of the cardiomyocyte's dynamic stability, the cell's recovery capability (restitution) following premature excitation was evaluated. The S1–S2 protocol [36], [37] was employed to construct APD restitution curves and analyze the phase portraits of electromechanical coupling. The protocol involved a series of 500 basal stimuli (S1) at a constant pacing frequency (basic cycle length of 1000 ms) to achieve a steady state of ionic concentrations. Subsequently, a single premature test stimulus (S2) was applied. The S1–S2 coupling interval was incrementally decreased with a step of 10 ms (and a finer step of 1–5 ms near the refractory threshold) until the loss of cellular excitability. Based on the obtained data, APD restitution curves were constructed, representing the dependence of the S2 test response (APD90) on the preceding diastolic interval (DI) (Fig. 9). This approach facilitated the identification of critical transition points from an adaptive physiological response to pathological membrane potential instability.

Under deep hypothermia (25 °C), the restitution curve exhibits high steepness. The maximum slope ( $S_{max}$ ) significantly exceeds the critical value of 1.0, reaching 1.35. According to the Nolasco–Dahlen criterion, such a state is a classic indicator of susceptibility to electrical alternans and the breakup of the excitation wave into fibrillatory rotors [38], [39]. Conversely, at 42 °C, despite the AP shortening, the restitution curve becomes flatter, and the slope approaches unity only at extremely short diastolic intervals (< 10 ms). Thus, hyperthermia partially "masks" electrical instability through accelerated repolarization, whereas hypothermia creates conditions for *re-entry* arrhythmias via steep restitution.

At 30 °C, the phase loops (Fig. 10) reflect a substantial alteration in the kinetics of excitation-contraction coupling. The trajectory is wide and elongated along the potential axis (the operating range, where calcium concentration remains elevated, spans  $\approx 102$  mV). The peak of the calcium transient (0.42  $\mu\text{M}$ ) is reached with a delay relative to the voltage peak, indicating preserved, albeit slowed, kinetics of calcium release from the sarcoplasmic reticulum [34], [40].

At 42 °C, a "compression" effect of the phase portrait is observed. The active voltage range narrows by 3.5 times (to  $\approx 28$  mV). However, the peak calcium concentration paradoxically increases to 0.44  $\mu\text{M}$ . Concurrently, the latency between depolarization and the calcium response is shortened. This indicates an "explosive" nature of calcium release: within the very short duration of the electrical pulse, the cell manages to mobilize a significant amount of ions, creating a risk of calcium overload even in the absence of overt electrical disturbances.

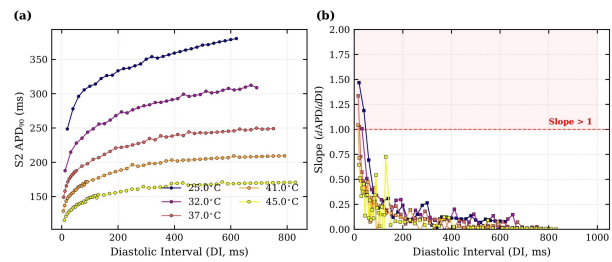


Fig. 9 APD restitution and stability across temperatures (25–45 °C): a) APD90 vs. DI curves; b) Corresponding restitution slopes. The red dashed line (Slope > 1) denotes the threshold for electrical alternans and wavebreak.

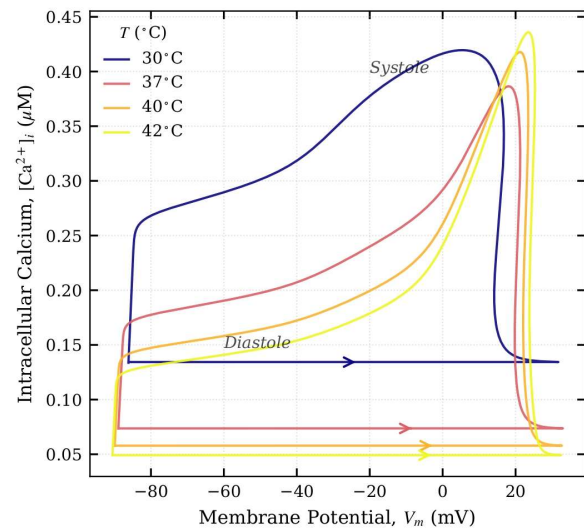


Fig. 10 Phase portraits ( $[Ca^{2+}]_i$  vs  $V_m$ ) demonstrating temperature-dependent modification of electromechanical coupling dynamics.

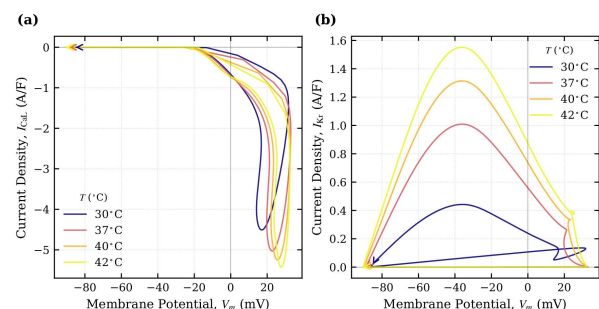


Fig. 11 Membrane potential – current density dynamic loops illustrating temperature-induced changes during the action-potential cycle: a)  $I_{CaL}$ ; b)  $I_{Kr}$ .

Dynamic analysis of ionic fluxes (Fig. 11) confirmed the mechanism of adaptive inversion in repolarization components. At 42 °C, the amplitude of  $I_{Kr}$  increased more than threefold compared with 30 °C, thereby providing robust repolarization and preventing critical AP prolongation. At the same time, the  $I_{CaL}$  current-voltage (I-V) loop shifted toward more positive potentials, indicating that hyperthermia intensifies calcium influx during the early phases of the AP. This explains the increased  $[Ca^{2+}]_i$  despite the shortened duration of the electrical pulse.

#### D. Validation of the Developed Model

Model validation was performed by comparing key electrophysiological characteristics of the AP with experimental data from human ventricular cardiomyocytes. To evaluate the electrophysiological changes, APD90 and  $(dV/dt)_{max}$  were selected as the primary evaluation metrics.

At the physiological temperature of 37 °C, the model exhibits an APD90 of 270.91 ms, which falls within the typical range of 270–310 ms reported for human ventricular cells in experimental studies and contemporary electrophysiological models [5], [29].

Upon decreasing the temperature to 25 °C, the APD90 reaches 413.07 ms, representing a 52.47% increase relative to the baseline state. Experimental research indicates that cooling cardiomyocytes from 37 °C to 25 °C leads to an AP prolongation of approximately 40–70% [12], [16], which is consistent with the simulation results.

Increasing the temperature to 42 °C results in a predicted APD90 shortening to 211.24 ms (a 22.03% decrease), aligning with established experimental observations of accelerated repolarization at elevated temperatures [41].

Furthermore, the model replicates the reduction in the maximum rate of depolarization during cooling:  $(dV/dt)_{max}$  decreases from 95.64 to 59.77 V/s. This effect is attributed to the slowing of sodium channel activation kinetics and is also in agreement with experimental findings [9], [12].

TABLE 2 COMPARISON OF SIMULATION RESULTS WITH LITERATURE DATA.

Temperature	APD90 (Model)	Change (%)	Experiment
25 °C	413.07 ms	52.47%	+40–70% [12], [16]
30 °C	359.55 ms	32.72%	Prolongation [12], [32]
37 °C	270.91 ms	baseline	270–310 ms [5], [29]
42 °C	211.24 ms	–22.03%	Shortening [41]

To quantitatively assess the consistency of the model results with experimental data, the relative deviation of APD90 changes from the mean of the experimental range was evaluated. For a temperature of 25 °C, the average experimental increase in APD is approximately 55% (within the 40–70% interval). The model's value of 52.47% corresponds to a deviation of approximately 4.6% from this mean value.

Such a deviation is considered negligible for biophysical models of cellular electrophysiology and indicates excellent agreement between the simulation results and experimental observations.

For additional verification of the developed parameter modification algorithm, a cross-model comparative analysis was performed, referencing the author's previous research [42]. In that work, analogous  $Q_{10}$  temperature coefficients were applied to the classic Luo-Rudy (LR) and Hodgkin-Huxley (HH) models (Fig. 12).

All models demonstrate a consistent qualitative temperature dependence: an increase in temperature results in a decrease in APD90 and an increase in  $(dV/dt)_{max}$ . Quantitative differences are attributed to the distinct parameterizations of ion channels and calcium handling mechanisms. The peak calcium transient is reproduced only in the modern model (ToR-ORd), whereas the Hodgkin-Huxley and Luo-Rudy models, in the configurations used, do not contain a detailed description of intracellular calcium dynamics. Overall, the results demonstrate a high degree of consistency between the proposed model and both experimental data and established biophysical models of cellular electrophysiology.

## IV. DISCUSSION

The obtained results underscore the complex, nonlinear nature of the temperature dependence of cardiomyocyte electrical activity [43]–[45]. The central conclusion

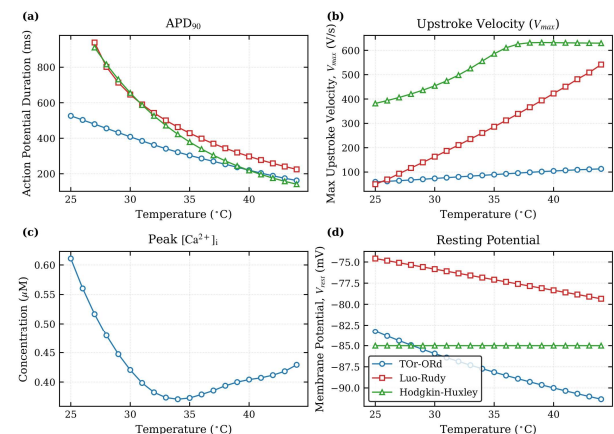


Fig. 12 Temperature dependence of ventricular cardiomyocyte electrophysiological properties predicted by different models. Comparison of the modified ToR-ORd model with previously modified Luo-Rudy and Hodgkin-Huxley models: a) APD90; b)  $(dV/dt)_{max}$ ; c)  $[Ca^{2+}]_i$ ; d) RPM.



of this study is the fact that the mechanisms of cardiac rhythm destabilization under hypothermia (30 °C) and hyperthermia (42 °C) have fundamentally different biophysical origins, which requires a differentiated approach to understanding thermally induced pathologies [32].

The observed phenomenon of "role inversion" (the reversal of the sign of the effect on APD during hypo- and hyperthermia) for ion channels—specifically NCX and  $I_{NaL}$ —demonstrates that cellular thermal adaptation is not a simple linear shift in reaction rates [44]. The transition of NCX from an AP-shortening factor at 30 °C to a prolonging factor at 42 °C is explained by the altered balance between the temperature-dependent kinetics of the exchanger and the voltage-dependent ionic gradients.

Of particular note is the adaptive role of the rapid delayed rectifier potassium channels  $I_{Kr}$ . The 3.5-fold increase in  $I_{Kr}$  amplitude during hyperthermia acts as a powerful protective mechanism that prevents excessive AP prolongation and the occurrence of early afterdepolarizations (EADs), consistent with both *in silico* and cellular research findings [46], [47].

However, the high nonlinearity of the sodium current ( $I_{Na}$ ) at 42 °C, identified via the Morris method, indicates that this stability is fragile: any combination of hyperthermia with genetic mutations (e.g., Long QT Syndrome) or pharmacological interventions could lead to an unpredictable repolarization failure [47].

The most unexpected finding is the disruption of electromechanical coupling observed at 42 °C. Traditionally, AP shortening is thought to reduce the time for calcium entry. However, the phase portrait data demonstrate the opposite: despite a critically short AP, an "explosive" increase in the  $[Ca^{2+}]_i$  peak to 0.44  $\mu\text{M}$  occurs [32], [48].

This phenomenon can be explained by a combined effect of altered  $I_{CaL}$  dynamics and disrupted calcium homeostasis. At elevated temperatures, the  $I_{CaL}$  current-voltage loop shifts toward more positive potentials, which promotes more intensive calcium influx during the early phases of depolarization. At the same time, compression of the phase loop along the voltage axis, together with preserved high calcium amplitude, suggests that the cell loses part of its ability to regulate calcium release from the sarcoplasmic reticulum adequately. This may be associated with accelerated RyR-mediated release and SERCA-dependent calcium cycling.

This establishes a specific mechanism of arrhythmogenesis during fever: triggered activity takes precedence over *re-entry*. Calcium overload at high heart rates can provoke delayed afterdepolarizations (DADs).

Despite the statistically significant results, several methodological limitations should be acknowledged:

- Absence of direct experimental verification: Due to the scarcity of data on the activity of isolated human cardiomyocytes at 30 °C and 42 °C, the model's systemic response is a result of mathematical extrapolation.
- Heterogeneity of  $Q_{10}$  sources: The temperature coefficients were sourced from various studies where they were calculated for isolated ion channels. The question of their collective adequacy within the dynamic environment of a whole cell remains open.
- Variability in literature data: Discrepancies in  $Q_{10}$  values across the literature, arising from different experimental methodologies, may be amplified by the nonlinear nature of the model.
- Simplification in sensitivity analysis: The Morris method serves as a qualitative screening tool. The application of more precise global sensitivity methods (e.g., Sobol' indices [44]) was limited by their high computational burden.
- Model isolation: This study describes a single epicardial myocyte and does not take into account intercellular interactions via junctions or the inherent heterogeneity of the myocardium (e.g., transmural gradients).

## CONCLUSIONS

As a result of this study, a temperature-dependent modification of the ToR-Ord model was developed, accounting for the effects of temperature on key ion channels, pumps, and exchangers. Proposed modification of the model facilitated a more detailed description of the electrophysiological behavior of human ventricular cardiomyocytes under temperature deviations from physiological norms. Sensitivity analysis identified the predominant in the model parameters responsible for AP thermal regulation. It was established that the primary determinant of repolarization duration adaptation is the rapid delayed rectifier potassium current  $I_{Kr}$ . Its contribution to the total reduction of APD90 during hyperthermia amounts to 84.62%, underscoring the critical role of Ether-à-go-go-Related Gene (hERG) channels in maintaining myocardial electrical stability.

It has been demonstrated that the influence of key ionic mechanisms on AP duration fundamentally depends on the direction of the temperature deviation from the physiological norm. Mechanisms that contribute to AP shortening under hypothermia (e.g., NCX current) cause its prolongation under hyperthermia. The most stable and potent regulator of repolarization

across the entire investigated range (25–45 °C) was identified as the current  $I_{Kr}$ . Its amplitude at 42 °C increases 3.5-fold compared to the 30 °C regime, performing a key adaptive function in maintaining electrical stability.

It was established that under conditions of deep hypothermia (30 °C), the primary factor of arrhythmogenic risk is electrical instability, caused by a sharp increase in the steepness of the electrical restitution curve (S1–S2 protocol), where the maximum slope exceeds the critical threshold of 1.35. This creates a favorable substrate for the emergence of APD alternans and the subsequent breakup of the excitation wave by the *re-entry* mechanism. Conversely, during hyperthermia (42 °C), restitution remains relatively flat; however, the risk of mechanical and metabolic destabilization increases significantly due to the critical shortening of the diastolic interval and alterations in intracellular calcium dynamics.

Analysis of the phase portraits  $[Ca^{2+}]_i - V_m$  demonstrated that at 42 °C, a sharp compression of the phase

loop along the voltage axis occurs (by a factor of 3.5), accompanied by an increase in the peak free calcium concentration to 0.44  $\mu$ M. The shortening of the time latency between the voltage peak and the calcium transient indicates a transition to highly accelerated calcium homeostasis kinetics. This elevation in kinetics increases the probability of calcium overload and the emergence of focal triggered activity (extrasystoles), even when the electrical stability of the membrane remains relatively preserved.

Global sensitivity analysis using the Morris method confirmed that under extreme hyperthermia, fast sodium channels ( $I_{Na}$  and their kinetic parameters) transition into a high-nonlinearity regime, where the nonlinearity index  $\sigma$  is three times greater than the mean of the absolute elementary effects  $\mu^*$ . This indicates that at high temperatures, the cell's electrical response becomes less predictable and highly sensitive to background fluctuations in other ionic currents.

## REFERENCES

- [1] Stefanu Buzatu, "The temperature-induced changes in membrane potential - PubMed," *Riv Biol*, vol. 102(2), pp. 199–217, 2009, PMID: 20077389.
- [2] J. Chi et al., "Hygrothermal stress increases malignant arrhythmias susceptibility by inhibiting the LKB1-AMPK-Cx43 pathway," *Scientific Reports* 2024 14:1, vol. 14, no. 1, pp. 5010–, Feb. 2024, PMID: 38424223.
- [3] M. Zaltieri, C. Massaroni, F. M. Cauti, and E. Schena, "Techniques for Temperature Monitoring of Myocardial Tissue Undergoing Radiofrequency Ablation Treatments: An Overview," *Sensors* 2021, Vol. 21, Page 1453, vol. 21, no. 4, p. 1453, Feb. 2021, PMID: 33669692.
- [4] J. Liu et al., "Heat exposure and cardiovascular health outcomes: a systematic review and meta-analysis," *Lancet Planet. Health*, vol. 6, no. 6, pp. e484–e495, Jun. 2022, PMID: 35709806.
- [5] J. Tomek et al., "Development, calibration, and validation of a novel human ventricular myocyte model in health, disease, and drug block," *Elife*, vol. 8, Dec. 2019, PMID: 31868580.
- [6] F. Yang and J. Zheng, "High temperature sensitivity is intrinsic to voltage-gated potassium channels," *Elife*, vol. 3, p. e03255, 2014, PMID: 25030910.
- [7] T. J. A. Allen, "Temperature dependence of macroscopic L-type calcium channel currents in single guinea pig ventricular myocytes," *J. Cardiovasc. Electrophysiol.*, vol. 7, no. 4, pp. 307–321, 1996, PMID: 8777479.
- [8] M. R. Tanner and C. Beeton, "Differences in ion channel phenotype and function between humans and animal models," *Front. Biosci. (Landmark Ed)*, vol. 23, no. 1, pp. 43–64, 2018, PMID: 28930537.
- [9] Bertil. Hille, *Ion channels of excitable membranes*. Sinauer Associates, Inc. ; Oxford University Press, 2001. ISBN: 9780197583074
- [10] T. Milburn, D. A. Saint, and S. H. Chung, "The temperature dependence of conductance of the sodium channel: implications for mechanisms of ion permeation," *Recept. Channels*, vol. 3, no. 3, pp. 201–211, 1995, PMID: 8821793.
- [11] T. Nagatomo et al., "Temperature dependence of early and late currents in human cardiac wild-type and long Q-T  $\Delta$ KPQ Na<sup>+</sup> channels," <https://doi.org/10.1152/ajpheart.1998.275.6.H2016>, vol. 275, no. 6 44–6, 1998, PMID: 9843800.
- [12] M. Vornanen, H. A. Shiels, and A. P. Farrell, "Plasticity of excitation–contraction coupling in fish cardiac myocytes," *Comp. Biochem. Physiol. A Mol. Integr. Physiol.*, vol. 132, no. 4, pp. 827–846, Aug. 2002, PMID: 12095866.
- [13] V. A. Maltsev and A. I. Undrovinas, "A Multi-Modal Composition of the Late Na<sup>+</sup> Current in Human Ventricular Cardiomyocytes," *Cardiovasc. Res.*, vol. 69, no. 1, p. 116, Jan. 2005, PMID: 16223473.
- [14] M. Mauerhöfer and C. K. Bauer, "Effects of Temperature on Heteromeric Kv11.1a/1b and Kv11.3 Channels," *Biophys. J.*, vol. 111, no. 3, pp. 504–523, Aug. 2016, PMID: 27508435.
- [15] M. Q. Dong, C. P. Lau, Z. Gao, G. N. Tseng, and G. R. Li, "Characterization of recombinant human cardiac KCNQ1/KCNE1 channels (I (Ks)) stably expressed in HEK 293 cells," *J. Membr. Biol.*, vol. 210, no. 3, pp. 183–192, Mar. 2006, PMID: 16909339.
- [16] T. Kiyosue, M. Arita, H. Muramatsu, A. J. Spindler, and D. Noble, "Ionic mechanisms of action potential prolongation at low temperature in guinea-pig ventricular myocytes," *J. Physiol.*, vol. 468, no. 1, pp. 85–106, Aug. 1993, PMID: 8254536.
- [17] S. Radicke et al., "Accessory subunits alter the temperature sensitivity of Kv4.3 channel complexes," *J. Mol. Cell. Cardiol.*, vol. 56, pp. 8–18, Mar. 2013, DOI: 10.1016/j.yjmcc.2012.12.017.
- [18] K. H. W. J. Ten Tusscher, D. Noble, P. J. Noble, and A. V. Panfilov, "A model for human ventricular tissue," <https://doi.org/10.1152/ajpheart.00794.2003>, vol. 286, no. 4 55–4, pp. 1573–1589, 2004, PMID: 14656705.
- [19] J. Millet et al., "Thermal modulation of epicardial Ca<sup>2+</sup> dynamics uncovers molecular mechanisms of Ca<sup>2+</sup> alternans," *Journal of General Physiology*, vol. 153, no. 2, Feb. 2021, PMID: 33410862.
- [20] Y. Nakamura, Y. Ohya, I. Abe, and M. Fujishima, "Sodium-potassium pump current in smooth muscle cells from mesenteric resistance arteries of the guinea-pig," *J. Physiol.*, vol. 519, no. Pt 1, p. 203, Aug. 1999, PMID: 10432351.
- [21] C. L. Elias, X. H. Xue, C. R. Marshall, A. Omelchenko, L. V. Hryshko, and G. F. Tibbits, "Temperature dependence of cloned mammalian and salmonid cardiac Na<sup>+</sup>/Ca<sup>2+</sup> exchanger isoforms," <https://doi.org/10.1152/ajpcell.2001.281.3.C993>, vol. 281, no. 3 50–3, 2001, PMID: 11502576.




- [22] Z. Zhou et al., "Properties of HERG channels stably expressed in HEK 293 cells studied at physiological temperature," *Biophys. J.*, vol. 74, no. 1, p. 230, 1998, PMID: 9449325.
- [23] J. I. Vandenberg, M. D. Perry, M. J. Perrin, S. A. Mann, Y. Ke, and A. P. Hill, "hERG K(+) channels: structure, function, and clinical significance," *Physiol. Rev.*, vol. 92, no. 3, pp. 1393–1478, 2012, PMID: 22988594.
- [24] B. Pahlavan, N. Buitrago, and F. Santamaria, "Macromolecular rate theory explains the temperature dependence of membrane conductance kinetics," *Biophys. J.*, vol. 122, no. 3, pp. 522–532, Feb. 2023, PMID: 36567527.
- [25] R. M. Daniel and M. J. Danson, "Temperature and the catalytic activity of enzymes: a fresh understanding," *FEBS Lett.*, vol. 587, no. 17, pp. 2738–2743, Sep. 2013, PMID: 23810865.
- [26] M. Clerx, P. Collins, E. de Lange, and P. G. A. Volders, "Myokit: A simple interface to cardiac cellular electrophysiology," *Prog. Biophys. Mol. Biol.*, vol. 120, no. 1–3, pp. 100–114, Jan. 2016, PMID: 26721671.
- [27] A. C. Hindmarsh et al., "SUNDIALS: Suite of nonlinear and differential/algebraic equation solvers," *ACM Transactions on Mathematical Software*, vol. 31, no. 3, pp. 363–396, 2005, DOI: 10.1145/1089014.1089020.
- [28] A. X. Sarkar and E. A. Sobie, "Regression Analysis for Constraining Free Parameters in Electrophysiological Models of Cardiac Cells," *PLoS Comput. Biol.*, vol. 6, no. 9, p. e1000914, 2010, PMID: 20824123.
- [29] T. O'Hara, L. Virág, A. Varró, and Y. Rudy, "Simulation of the Undiseased Human Cardiac Ventricular Action Potential: Model Formulation and Experimental Validation," *PLoS Comput. Biol.*, vol. 7, no. 5, p. e1002061, 2011, PMID: 21637795.
- [30] E. A. Sobie, "Parameter sensitivity analysis in electrophysiological models using multivariable regression," *Biophys. J.*, vol. 96, no. 4, pp. 1264–1274, Feb. 2009, PMID: 19217846.
- [31] M. Balesdent, L. Brevaux, S. Lacaze, S. Missoum, and J. Morio, "Methods for high-dimensional and computationally intensive models," *Estimation of Rare Event Probabilities in Complex Aerospace and Other Systems: A Practical Approach*, pp. 109–136, 2016, DOI: 10.1016/B978-0-08-100091-5.00008-3.
- [32] E. S. Dietrichs et al., "Moderate but not severe hypothermia causes pro-arrhythmic changes in cardiac electrophysiology," *Cardiovasc. Res.*, vol. 116, no. 13, p. 2081, Nov. 2020, PMID: 32031595.
- [33] M. Aguilar and S. Nattel, "The pioneering work of George Mines on cardiac arrhythmias: groundbreaking ideas that remain influential in contemporary cardiac electrophysiology," *J. Physiol.*, vol. 594, no. 9, p. 2377, May 2016, PMID: 26607760.
- [34] A. Crispino et al., "A cross species thermoelectric and spatiotemporal analysis of alternans in live explanted hearts using dual voltage-calcium fluorescence optical mapping," *Physiol. Meas.*, vol. 45, no. 6, p. 065001, Jun. 2024, PMID: 38772394.
- [35] H. Olai et al., "Meta-analysis of targeted temperature management in animal models of cardiac arrest," *Intensive Care Medicine Experimental* 2020 8:1, vol. 8, no. 1, pp. 3–, Jan. 2020, PMID: 31953652.
- [36] G. Tse, S. T. Wong, V. Tse, and J. M. Yeo, "Restitution analysis of alternans using dynamic pacing and its comparison with S1S2 restitution in heptanol-treated, hypokalaemic Langendorff-perfused mouse hearts," *Biomed. Rep.*, vol. 4, no. 6, p. 673, Jun. 2016, PMID: 27284405.
- [37] "Dynamic and S1S2 restitution curves in the three model versions. Each... | Download Scientific Diagram." [Online]. Available: [https://www.researchgate.net/figure/Dynamic-and-S1S2-restitution-curves-in-the-three-model-versions-Each-panel-represents\\_fig6\\_221683402](https://www.researchgate.net/figure/Dynamic-and-S1S2-restitution-curves-in-the-three-model-versions-Each-panel-represents_fig6_221683402). [Accessed: 10-Mar-2026].
- [38] A. Loppini, A. Barone, A. Gizzi, C. Cherubini, F. H. Fenton, and S. Filippi, "Thermal effects on cardiac alternans onset and development: A spatiotemporal correlation analysis," *Phys. Rev. E*, vol. 103, no. 4, p. L040201, Apr. 2021, PMID: 34005953.
- [39] R. Majumder, A. Nabizath, M. Nazer, A. V Panfilov, E. Bodenschatz, and Y. Wang, "Electrophysiological characterization of human atria: the understated role of temperature," *bioRxiv*, p. 2020.12.07.414573, Dec. 2020, DOI: 10.1101/2020.12.07.414573.
- [40] B. Hegyi et al., "Altered Repolarization Reserve in Failing Rabbit Ventricular Myocytes: Calcium and  $\beta$ -Adrenergic Effects on Delayed- and Inward-Rectifier Potassium Currents," *Circ. Arrhythm. Electrophysiol.*, vol. 11, no. 2, Feb. 2018, PMID: 29437761.
- [41] Y. Zhao and J. A. Boulant, "Temperature effects on neuronal membrane potentials and inward currents in rat hypothalamic tissue slices," *J. Physiol.*, vol. 564, no. Pt 1, pp. 245–257, Apr. 2005, PMID: 15695248.
- [42] V. O. Ivashchuk, "Modelyuvannya vplyvu temperatury na elektrychnu aktyvnist' sertseyvkh klityn [Modeling the influence of temperature on the electrical activity of heart cells]." Igor Sikorsky KPI, 2024, URL: <https://ela.kpi.ua/handle/123456789/67891>
- [43] Y. Belhamadia and J. Grenier, "Modeling and simulation of hypothermia effects on cardiac electrical dynamics," *PLoS One*, vol. 14, no. 5, p. e0216058, May 2019, PMID: 31050665.
- [44] P. P. Kanade, N. E. Ouyunbaatar, and D. W. Lee, "Effects of low temperature on electrophysiology and mechanophysiology of human induced pluripotent stem cell-derived cardiomyocytes (hiPSC-CMs)," *Micro and Nano Systems Letters* 2021 9:1, vol. 9, no. 1, pp. 9–, Oct. 2021, DOI: 10.1186/s40486-021-00135-2.
- [45] S. Meier, A. Grundland, D. Dobrev, P. G. A. Volders, and J. Heijman, "In-silico analysis of the dynamic regulation of cardiac electrophysiology by Kv11.1 ion-channel trafficking," *J. Physiol.*, vol. 601, no. 13, p. 2711, Jul. 2023, PMID: 36752166.
- [46] M. Varshneya, R. A. Devenyi, and E. A. Sobie, "Slow Delayed Rectifier Current Protects Ventricular Myocytes From Arrhythmic Dynamics Across Multiple Species," *Circ. Arrhythm. Electrophysiol.*, vol. 11, no. 10, p. e006558, Oct. 2018, PMID: 30354408.
- [47] B. Hegyi et al., "Balance Between Rapid Delayed Rectifier K+ Current and Late Na+ Current on Ventricular Repolarization: An Effective Anti-arrhythmic Target?," *Circ. Arrhythm. Electrophysiol.*, vol. 13, no. 4, p. E008130, Apr. 2020, PMID: 32202931.
- [48] A. Varró et al., "Cardiac transmembrane ion channels and action potentials: cellular physiology and arrhythmogenic behavior," *Physiol. Rev.*, vol. 101, no. 3, pp. 1083–1176, Jul. 2021, PMID: 33118864.

Надійшла до редакції 30 березня 2026 року  
 Прийнята до друку 25 квітня 2026 року  
 Опублікована 04 травня 2026 року.




# Моделювання впливу температури на електричну активність серцевих клітин: ідентифікація ключових іонних струмів за допомогою аналізу чутливості

В. О. Івашук<sup>f</sup>,  [0009-0004-2687-9188](https://orcid.org/0009-0004-2687-9188)

Н. Г. Іванушкіна<sup>g</sup>, канд. техн. Наук, доц.,  [0000-0001-8389-7906](https://orcid.org/0000-0001-8389-7906)

Національний технічний університет України

"Київський політехнічний інститут імені Ігоря Сікорського"  [00syn5v21](https://doi.org/10.20535/2523-4455.me.357181)  
Київ, Україна

**Анотація**— У роботі представлено розробку модифікованої електрофізіологічної моделі епікардіального кардіоміоцита людини з урахуванням температурного впливу на кінетику та провідність іонних каналів за допомогою параметрично-специфічних коефіцієнтів  $Q_{10}$ . На основі модифікованої моделі виконано аналіз температурної чутливості для визначення ключових іонних механізмів, що регулюють температурну адаптацію тривалості потенціалу дії (APD). Моделювання виконано в діапазоні температур 25–45 °C із використанням гібридного підходу, що поєднує локальний і глобальний аналізи чутливості. Локальний аналіз здійснено шляхом розрахунку коефіцієнтів еластичності для оцінювання впливу окремих температурних параметрів на APD. Глобальний аналіз проведено з використанням методу елементарних ефектів Морріса для ранжування параметрів за їхнім впливом та виявлення нелінійних взаємодій.

Результати показали, що швидкий калієвий струм затриманого випрямлення (IKr) відіграє переважну роль у модуляції APD. На нього припадає приблизно 85% загального скорочення APD при підвищенні температури до 42 °C, де тривалість потенціалу дії зменшується на 22,03% (з 270,91 мс до 211,24 мс). За умов глибокої гіпотермії (25 °C) спостерігалось подовження потенціалу дії на 52,47% та збільшення тривалості фази реполяризації на 169%. Крім того, дослідження виявило, що при помірній гіпотермії (30 °C) вирішальним фактором стають нелінійні взаємодії між різними іонними каналами. Було продемонстровано значний внесок натрій-кальцієвого обмінника (NCX) та пізнього натрієвого струму (INaL) при низьких температурах, що підтверджує температурну залежність цих взаємодій. Отримані результати підкреслюють критичну роль людського гену *Ether-à-go-go-Related Gene* (hERG) у термічній адаптації міокарда шлуночків і створюють розрахункову базу для вивчення механізмів виникнення термоіндукованих аритмій.

**Ключові слова** — температурні ефекти; електрофізіологія серця; аналіз чутливості; метод Морріса; коефіцієнти  $Q_{10}$ ; потенціал дії; іонні канали.

